NANO LETTERS

2009
Vol. 9, No. 7
2683-2689

Selective Sputtering and Atomic Resolution Imaging of Atomically Thin Boron Nitride Membranes

Jannik C. Meyer,* Andrey Chuvilin, Gerardo Algara-Siller, Johannes Biskupek, and Ute Kaiser*

Electron Microscopy of Materials Science, University of Ulm, 89069 Ulm, Germany

Received April 9, 2009; Revised Manuscript Received May 14, 2009

ABSTRACT

We report on the preparation, atomic resolution imaging, and element selective damage mechanism in atomically thin boron nitride membranes. Flakes of less than 10 layers are prepared by mechanical cleavage and are thinned down to single layers in a high-energy electron beam. At our beam energies, we observe a highly selective sputtering of only one of the elements and predominantly at the exit surface of the specimen, and then subsequent removal of atoms next to a defect. Triangle-shaped holes appear in accordance with the crystallographic orientation of each layer. Defects are compared to those observed in graphene membranes. The observation of clean single-layer membranes shows that hexagonal boron nitride is a further material (in addition to graphene) that can exist in a quasi-two-dimensional allotrope without the need for a substrate.

Experimental surface science and the science of low-dimensional systems have experienced a change in paradigm with the isolation of graphene,[1−4] a single layer of carbon atoms that exists without the need for a substrate with matching lattice. Single-layer graphene has outstanding electronic properties that, in essence, are a consequence of it having a different symmetry than its bulk counterpart (graphite).[5] Graphene can even exist as free-standing membrane, thus exposing two surfaces from the same set of atoms,[6−9] and is the only material that has been obtained as sizable suspended one-atom-thick foils so far. Here, we present single-layer membranes of hexagonal boron nitride, a structurally similar material with yet entirely different properties.

The structural variety of boron nitrides is very similar to that of carbon solids: Diamond-like cubic boron nitride (c-BN) and graphitic hexagonal boron nitride (h-BN), sometimes called white graphite, constitute the common three-dimensional phases, while BN nanotubes[10−14] and fullerenes[15,16] constitute lower dimensional solid phases. Also the chemistry of boron−nitrogen systems appears to be quite rich,[17] albeit somewhat less explored than that of organic compounds. Single layers of boron nitride have been obtained previously by decomposition of borazine on metal surfaces with a matching lattice,[18] in a mesh structure in the case of a lattice mismatch,[19] or in folded shapes by solution processing of h-BN.[20] We present here the experimental observation of single-layer hexagonal boron nitride in free-standing membranes up to a few nanometers in size. The membranes and their defects are studied by aberration-corrected transmission electron microscopy. Defect dynamics in BN layers are compared to those in graphene sheets. The 3-fold symmetry of single boron nitride layers, along with an asymmetric damage mechanism, leads to the formation of triangle-shaped holes in the electron beam.

The first part of the sample preparation, resulting in ultrathin membranes of hexagonal boron nitride layers (10 atomic layers or less), follows the procedure reported in ref 21 with small differences. Hexagonal boron nitride powders with a large average crystal size of 10−15 μm (Grade AC6004 from Henze boron nitride products GmbH, or grade S15 from ESK Ceramics GmbH) are placed onto an adhesive tape, peeled apart several times, and then rubbed on a silicon wafer with a 300 nm silicon oxide layer. Thin flakes are located in an optical microscope (OM) (Figure 1a). A Quantifoil TEM grid (1.3 μm holes, 200 mesh gold grid) is placed on the flake. A drop of solvent (isopropanol) is added and allowed to evaporate. The surface tension pulls the carbon film of the TEM grid into close contact with the silicon oxide surface.[22] Heating on a hot plate (200 °C, 20 min.) improves the contact between the grid and the flakes. A precursor of polyimide, called poly(pyromellitic dianhydride-*co*-4,4′-oxidianiline) (or amic acid) 15% solution in methylpyrrolidone, is dropped onto the sample and baked at 115 °C for 15 min. After polymerization, the polyimide along with the TEM grid and BN flakes is peeled off from

* Authors to whom correspondence should be addressed: E-mail: email@jannikmeyer.de (J.C.M.) and ute.kaiser@uni-ulm.de (U.K.).

10.1021/nl9011497 CCC: $40.75
Published on Web 05/29/2009

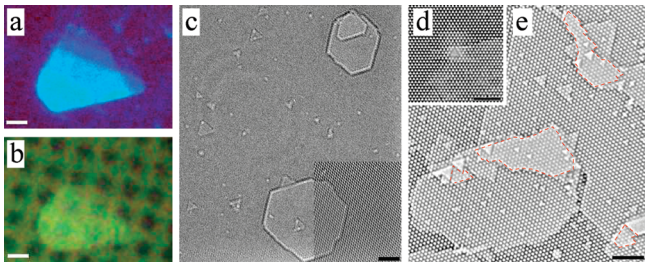

Figure 1. Preparation of single-layer hexagonal boron nitride membranes. (a) Optical micrograph of a few-layer BN flake on the silicon substrate, with its thinnest region at the upper right edge. (b) The same flake after transfer to the Quantifoil grid (the thinnest regions are not visible). (c−e) High-resolution TEM images. (c) Initial view after brief irradiation on the thinnest part. Small triangle-shaped holes appear where the thickness is reduced by one layer, while larger holes exhibit irregular polygon shapes and thickness reduction of more than one layer. The lattice contrast is filtered out (a part of the original image is shown in the lower right corner). (d) After 35 min of electron irradiation, a first isolated hole appears. (e) Formation of single-layer h-BN membranes, indicated by red dashed regions, after slightly more irradiation (ca. 1 min after the first hole). Scale bars 2 μm (a and b), 2 nm (c−e).

the substrate in one piece. After the polyimide is dissolved (in a 60 °C methylpyrrolidone bath, for 2 h), the TEM grid with the flakes is transferred to isopropanol and dried in air (Figure 1b). OM images are recorded during this preparation in order to find the same flakes in the transmisson electron microscope (TEM). The above method results in few-layer hexagonal boron nitride membranes with a uniform thickness across several micrometers. However, we did not succeed in obtaining single-layer boron nitride samples by mechanical cleavage with adhesive tape, as is the case for graphene.

Further thinning is performed in situ in the TEM. We use an FEI Titan 80-300 TEM equipped with an imaging aberration corrector, operated at 80 kV. In a first step, a high current density beam (ca. 1×10^8 $e^-/(s{\cdot}nm^2)$) is produced on the sample, sputtering off subsequent layers one by one from the boron nitride membranes. It is the high anisotropy of this process that allows us to obtain single-layer regions of several nanometers in size: Holes "grow" predominantly within a given layer, while the ajacent next layer remains stable for a sufficient amount of time. Figure 1c shows an almost-initial configuration where the beam damage has just started to form small holes, locally reducing the thickness by one or two layers. The entire thinning is shown in supplementary video S1 in the Supporting Information. As soon as a hole through the entire thickness appears (Figure 1d), the conditions are tuned for optimum imaging with lower current density (ca. 2×10^7 $e^-/(s{\cdot}nm^2)$). After some more irradiation, single-layer h-BN membranes can be found within the irradiated regions (Figure 1e). Since this thinning is observed in real time, the process could easily be stopped by switching off the electron beam after formation of the first hole (Figure 1c) or potentially at the first vacancy through the entire sheet. In such a way, a precisely defined nanopore can be formed in a stable, insulating membrane that may find use in, e.g., DNA translocation experiments,[23] as a nonround molecular filter, or as a precisely defined aperture or shadow mask with atomically sharp edges. For example, the triangle-shaped hole in Figure 1c has an edge length of only 7 Å, and grows to 30 Å before a second hole is formed in the same membrane.

For comparison, graphene membranes were prepared as described in refs 22 and 24. Graphene has an almost identical lattice constant (in-plane 2.46 Å for graphene and 2.50 Å for h-BN). Boron, nitrogen, and carbon produce a nearly identical contrast in high-resolution TEM images, according to image simulations; thus, the observations are easily comparable. Thinning from a few layers to a single layer under electron irradiation can be observed in graphite too. However, it is more convenient, and results in much larger single-layer areas, to prepare single-layer graphene membranes directly.

For atomic resolution imaging, we use spherical aberrations (C_s) between 18 and 26 μm, with a defocus corresponding to about 1.3 times the Scherzer defocus.[25] At these conditions, atoms appear black. A noticeable improvement of contrast and spatial resolution, both of which are limited by chromatic aberration at this low voltage, is obtained by reducing the extraction voltage from its standard value (3.8 kV) to 1.7 kV and thus reducing the energy spread of the source.[26] The full width at half-maximum of the zero-loss peak in the electron energy loss spectrum is now reduced by ca. 0.2 eV. The second set of reflections in the Fourier transform (FT) of high-resolution images from single layers, corresponding to 1.25 Å for h-BN and 1.23 Å for graphene, becomes visible (Figure 2d,e) and the separation of B−N or C−C atoms is resolved in the image (Figure 2d). Only weak filtering is applied: The effects of a slightly uneven illumination intensity in the images are removed by a high-pass filter with a smooth cutoff at 2 nm (removing only longer-range intensity variations), and smoothing (by a Gaussian blur) to a resolution of ca. 1 Å is done. Single exposures (1 s) provide sufficient signal to detect individual B, C, or N atoms or individual vacancies (Figure 4c) above the noise. Single exposures are shown in Figure 4 in order to resolve the dynamics. Figures 1, 2, and 3 show averaged images from between 3 and 10 exposures to improve the signal-to-noise ratio; however, we verified that the features of interest did not change during the respective part of the image sequence. The supplementary videos in Supporting Information show single exposures in each frame.

The experiment begins with few-layer membranes and ends with the observation of single-layer boron nitride regions. However, for a clear and straightforward understanding, we begin our discussion with the single-layer regions. Figure 2a shows a large single-layer boron nitride layer surrounded by holes and few-layer regions. A comparison with single-layer graphene membranes (Figure 2b), imaged at the same conditions, is shown as difference image (Figure 2c) and in the profile plots (Figure 2d). The presence of one single layer of h-BN is established by each of the following points: (1) The intensity of the lattice contrast changes in discrete units with the removal of subsequent layers, and the single layer region produces precisely that unit of contrast (Figure 2d). (2) The removal of the last layer results in a hole (vacuum), and also monovacancies in this

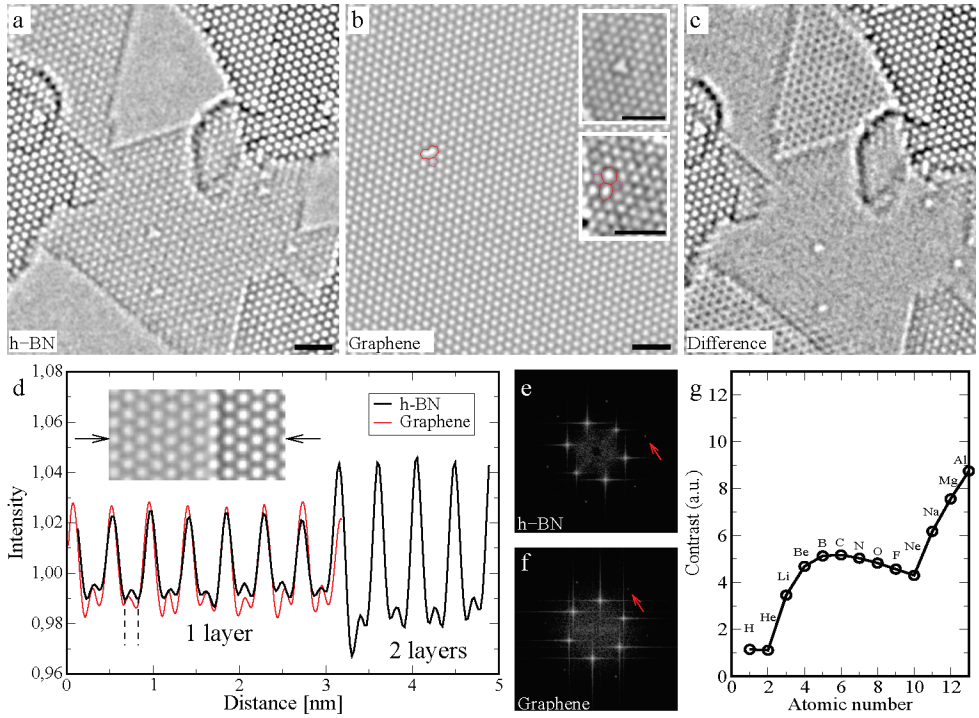

Figure 2. Comparison of h-BN and graphene membranes. (a) h-BN membrane and (b) single-layer graphene membrane HRTEM images at 80 keV. The single-layer h-BN region in (a) is the region with light-gray lattice contrast that fills the largest part of the image, including a few monovacancies and larger triangle-shaped holes. In contrast, (b) shows a reconstructed vacancy in a single-layer graphene sheet. We also observe nonreconstructed vacancies (upper inset) and Stone−Wales defects (lower inset) in graphene. (c) Numerical difference of the graphene and h-BN image (alignment by a scaled rotation). (d) Intensity profiles from lattice images of h-BN and graphene membranes. Single-layer regions produce an essentially identical contrast. The B−N and C−C separation is clearly resolved (dashed lines). The inset shows the h-BN image where the profile was taken, across a step edge from one to two layers. (e) Fourier transform (log scale) of an h-BN lattice image, with a thickness between one and three layers in the chosen area. (f) Fourier transform (log scale) for a graphene lattice image, taken from a "perfect" single-layer region with no adsorbates or defects. In both cases, the second reflections at 1.26 Å (h-BN) and 1.23 Å (graphene) are clearly present (red arrows). (g) Calculated contrast of several light elements for bright-field TEM. No significant contrast difference for B, C, and N is expected, in agreement with our experiment (see panels c and d). All scale bars are 1 nm.

layer clearly have no second atom beneath. (3) The contrast is identical to that of single-layer graphene observed at the same conditions (Figure 2c,d; in the graphene samples with their larger areas, the presence of one single layer can be unambiguously shown by electron diffraction).[6,7,27] (4) The behavior of hole growth from defects (described below) is in agreement with only the structure and symmetry of single h-BN layers. The evolution of the structure, hole growth from vacancies, and other beam-induced dynamics in single-, double-, and triple-layer hexagonal boron nitride is also shown in supplementary video S2 in Supporting Information.

First, we compare point defects, observed in isolated boron nitride layers, to those observed in graphene membranes at identical conditions. Figure 2a (also Figures 1e, 3a, and 4c) shows a number of monovacancies in single-layer h-BN that are readily apparent as a triangle-shaped white spot. In h-BN layers, monovacancies exclusively appear in this nonreconstructed configuration (i.e., no rearrangement after removal of an atom) with a 3-fold symmetry. Figure 2b and the upper inset show two images of a vacancy with one missing carbon atom in the graphene membrane.[28] One of them constitutes a simple monovacancy with no reconstruction, and the other one is a reconstructed vacancy that has formed a pentagon−nonagon pair. These two configurations are seen to convert from one type to another in both directions, and the reconstructed configuration is observed more frequently. The second inset in Figure 2b shows a Stone−Wales defect.[29−31] Neither the reconstructed vacancy nor a Stone−Wales type defect was observed in our h-BN membranes. Further, even after significant restructuring of h-BN edges such as shown in Figure 4, no such topological defects are seen. These results confirm that B−B or N−N bonds are highly unfavorable compared to the h-BN configuration,[11−13] while C−C bonds in a pentagon−heptagon or other odd-numbered ring configuration in graphene are readily generated under electron irradiation, especially at edges. Reconstructed vacancies have been observed in curved (tubular) h-BN structures[32] but not in planar h-BN sheets as demonstrated here; both observations are in agreement with calculations.[32] Thus, it appears that h-BN is another system where the curvature and topology, rather than only the local configuration, affects the shape and dynamics of defects.[31]

Another difference in comparison with graphene is seen in comparing images of single- and few-layer regions. Few-layer graphene maintains the bernal (AB) stacking sequence of graphite,[7] and thus, a bilayer has a qualitatively different appearance than a single layer (see Figure 2d,e of ref 31, note that in ref 31 atoms are white). In the case of hexagonal boron nitride, different stacking sequences were predicted to be stable in ref 33. Our data for few-layer h-BN are only

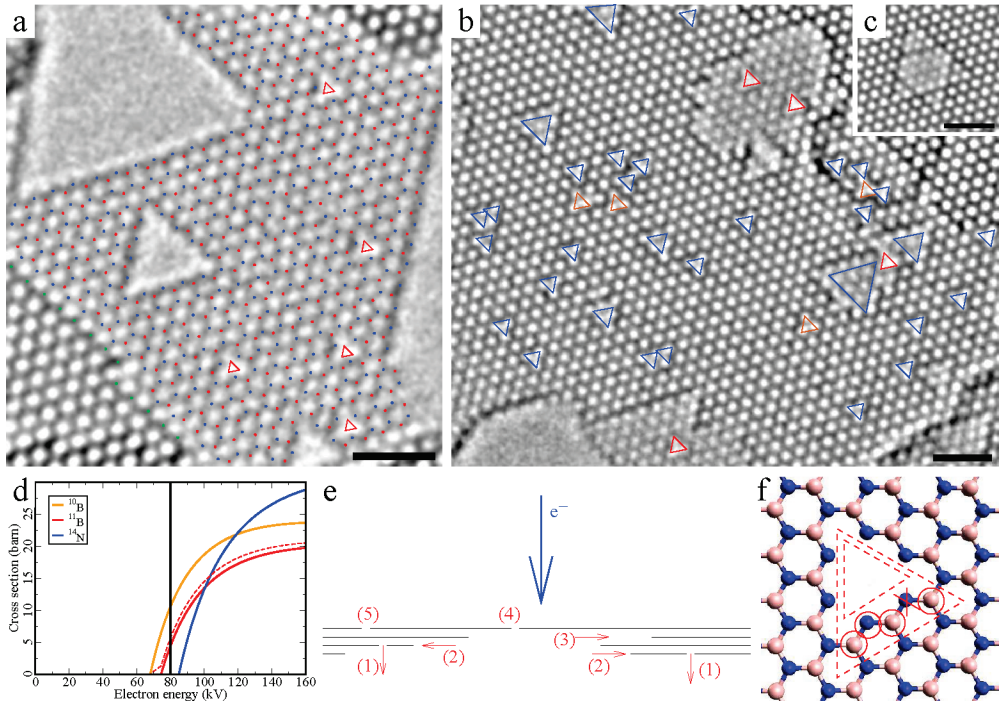

Figure 3. Radiation damage mechanism in h-BN membranes. (a) Single-layer h-BN membrane. All isolated vacancies (one missing atom; red triangles) exclusively appear on the same sublattice. The orientation of the triangle-shaped holes is maintained as the holes expand: The more stable element in the bulk (blue dots) is also the edge termination. Also the edge of the second layer (lower left corner, green dots) is terminated by the same element. (b) A mostly two-layer h-BN membrane in the same sample. Here, all single vacancies appear on the other sublattice (blue triangles), with few exceptions (brown). Red triangles are again vacancies in single-layer regions. (c) Triangles growing in opposite orientation in two adjacent layers of a three-layer h-BN membrane. (d) Total knock-on cross sections for B and N atoms vs electron energy for h-BN membranes. Red dashed line is the average, weighted by relative abundances, for the two B isotopes. (e) Schematic of the damage mechanism: (1) Individual atoms are sputtered off on the exit surface layer. (2) Holes grow from these defects, predominantly within the layer. (3) Edges can even recede behind an adjacent layer, as seen in panel (c). (4) Vacancy in the last layer. (5) Exception case of an atom sputtered off on the beam entrance surface, identified as such because it remains in the last layer at a later time. (f) Growth of oriented holes from vacancies. We start with the smaller triangle-shaped hole (inner dashed line), which is terminated with the blue atoms, and rather stable in the beam. After random removal of an edge atom (crossed out in red), all two-coordinated red and single-coordinated blue atoms that are formed in the process (red circles) are quickly removed too. The result is again a blue-atom terminated triangle-shaped hole with the same orientation (outer dashed line). Scale bars (a−c) are 1 nm.

consistent with one of them (structure "A" of ref 33), which is the structure of the bulk material. In this structure, the B atom of one layer is centered on the N atom of the next layer (and vice versa). Consequently, only the amount of contrast changes with the number of layers (Figure 2d).

We now look more closely at the defects in single-layer h-BN membranes. It is striking that all single vacancies are located on the same sublattice. This can be seen by counting along the lattice atoms (Figure 3a), and it is also evident in all images as the triangle-shaped white contrast of the defects having the same orientation (Figures 1e, 2a, 3a, and 4c). This correlation is maintained across separate single-layer areas of the same sample and single-layer regions formed at different times. Thus, all atoms that are knocked out from an unperturbed single-layer h-BN sheet by the electron beam must be of the same type—either boron or nitrogen.

Calculations of knock-on thresholds and cross sections in ref 34 suggest that boron is exclusively sputtered from h-BN sheet at an acceleration voltage of 80 kV. This calculation can also be understood from a simple argument: The maximum transferred energy in a collision between the electron and the nucleus depends on their relative masses. Thus, an 80 keV electron can transfer a maximum energy of 18.8 and 17.1 eV to the ^{10}B and ^{11}B isotopes, respectively, but only 13.4 eV to the ^{14}N atom.[35] Thus, if the threshold energies for atom knockout are similar for the two elements, then sputtering of exclusively the boron sites will occur within a suited range of acceleration voltages.

In order to test this interpretation, we have also looked at the radiation damage with acceleration voltages of 100 and 120 kV. At 120 kV, the maximum transferred energies are 29.2, 26.5, and 20.8 eV to the ^{10}B, ^{11}B, and ^{14}N nuclei, respectively. Experimentally, we find that the entire damage mechanism proceeds more rapidly at these higher voltages. However, we still find that exclusively only one of the elements forms a monovacancy on the h-BN surfaces and h-BN monolayers. This observation seems to be at odds with the calculated knock-on cross sections, which predict atom knockout of both elements at 100 and 120 kV. However, there might be other mechanisms in addition to the pure knock-on damage, such as an immediate replacement of the ejected atom from mobile atoms on the surface for one of the two elements.[36] Further, it is possible that only one type of vacancy is stable; if this is the case, then this should be the nitrogen vacancy according to earlier experiments.[37] In either case, we cannot be sure that it is the boron site which

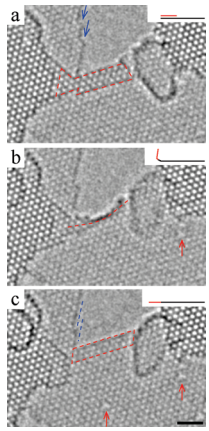

Figure 4. Dynamics in h-BN membranes. Red dashed line indicates a bilayer strip that unfolds into a single-layer region: (a) A bilayer region is indicated by the red dashed line. This area folds over and appears nearly parallel to the beam (b) during one exposure and (c) unfolds into the region of the large hole. The area indicated by the red dashed line in (c) was empty during frame (a). No topological defects are incorporated during this edge reconstruction. On the other edge of the same hole, atoms are removed by the electron beam. The lines of atoms indicated by the blue arrows recede, and the region indicated by blue dashed lines in (c) has been removed from (a) to (c). Also visible in the sequence is the generation of vacancies within the single-layer h-BN membrane, indicated by red arrows. Time between the images is 8 s. Scale bar, 1 nm.

is sputtered in our case. We will thus label, in the following, the ejected species as element 1 (red dots in Figure 3) and the more stable one as element 2 (blue dots in Figure 3). Unfortunately, even though the atomic spacing is resolved spatially (Figure 2d), the boron and nitrogen sites cannot be distinguished in a bright-field, high-resolution TEM image: Figure 2g shows the contrast for simulated single-atom images, using the code of ref 38. The actual value depends on imaging conditions; however the trend and nearly identical contrast of B, C, N, and oxygen does not change considerably (see also Figure 32 of ref 39) and there is also negligible difference in simulated lattice images. Moreover, the tiny difference that is found in the calculation depends sensitively on the imaging conditions and is easily dominated by residual aberrations if the atoms are arranged into a lattice. The experiment confirms the nearly identical contrast, also in comparison to graphene (Figure 2c,d).

Now we compare single-layer and bilayer regions in the same sample (Figure 3a,b): Going from one to two layers, it is immediately apparent that in the bilayer region, monovacancy defects appear predominantly (ca. 90%) on the *other* sublattice of the projected structure. If we consider again the structure—B is above N in subsequent layers—it is obvious that again the element 1 site is sputtered but now from the next layer. In the image (Figure 3b), this can be easily seen as the orientation of the triangle-shaped defect being rotated by 180° in single-layer vs bilayer regions. This trend continues layer by layer as we look at thicker regions. Therefore, the atoms that are ejected from few-layer regions again must be of the same type, and in addition from only one of the layers. In our scattering geometry—electrons at normal incidence to the membrane and largest momentum transfer in forward direction—this must be the exit surface of the specimen. There are a few exceptions (ca. 10% of the monovacancies) in the few-layer regions. At least part of these exceptions must be element 1 atoms sputtered off on the beam entrance surface, as they were found to remain after the region was thinned to one layer (Figure 3e). Overall, we conclude that there is a very high selectivity in sputtering exclusively only one of the two elements, predominantly at the exit surface, in hexagonal boron nitride membranes in the 80−120 keV electron beam.

Ajacent to vacancies in the membrane, the situation is evidently different: Atoms next to a vacancy or at the edges of larger holes are ejected regardless of their type, and at a higher rate. Again, there appears to be a peculiar and highly selective damage mechanism: Single vacancies "grow" within the respective layer into beautiful triangle-shaped holes. In particular, the triangle maintains its orientation, and again, triangle-shaped holes in adjacent layers display the opposite orientation. The resulting shapes resemble Sierpinski triangles with a minimum granularity given by atomic dimensions. Strong conclusions on the damage mechanism can be obtained also from this observation: If we assume similar probabilities for ejecting the two-coordinated B or N atoms at an edge or next to a vacancy, hexagon-shaped holes would have to appear. Only if we assume a strong asymmetry in the ejection probabilities, can the triangle-shaped holes be explained: Two-coordinated atoms of element 1 at an edge must be quite unstable, while the two-coordinated atoms of element 2 must be much more stable in the beam. In agreement, if we identify the element 1 sublattice (in single layers) based on vacancies, we see that the edges are element 2 terminated. Figure 3f illustrates the growth process of triangle-shaped holes. The rapid removal of a zigzag line, after the termination is broken at one point, can indeed be observed in the larger holes or at open edges (Figure 4) and is indicated by arrows in supplementary video S3 in Supporting Information.

In conclusion, we have shown the preparation and atomic resolution imaging of single-layer hexagonal boron nitride membranes by 80 kV Cs-corrected high-resolution transmission electron microscopy. Defects in these membranes are studied and compared to those observed in graphene membranes at identical conditions. No topological defects or vacancy reconstructions were observed in h-BN, confirming a disfavor of B−B or N−N bonds, while odd-numbered rings in the carbon system are readily formed. We obtain unprecedented insights into radiation damage in a high-energy electron beam. In particular, the high element selectivity of the radiation damage in this material is demonstrated. The observed damage mechanisms, i.e., selective atom removal, layer-by-layer sputtering, growth of triangle-shaped holes, and edge vs surface/bulk sputtering can be well understood in the picture of knock-on damage; however the energies differ from calculated values and additional mechanisms might be involved. In this context, it should be noted that hexagonal boron nitride is an insulator (or large band gap semiconductor) where one might expect ionization effects to be dominant. A few further pecularities

remain, for example, vacancies in one layer are generated more frequently just where an edge of the next layer is present.

A wealth of science and applications can be expected from single- and few-layer hexagonal boron nitride membranes. h-BN is a wide band gap material with outstanding mechanical, electrical and optical properties over a wide range of temperatures. The almost identical lattice constant with graphite or graphene suggests a joint use in composite devices. For silicon-based microelectronics, it was the existence of a good insulator−silicon dioxide−that favored this technology over other semiconductor materials, and BN layers might serve a simliar role in possible graphene-based devices. The use of h-BN as a template for graphene has been proposed in order to obtain a band gap in graphene.[40] Both h-BN layers and graphene have outstanding properties, have an almost identical lattice constant, and are stable as membranes of single-layer thickness. Structural modifications, including atomically sharp edges and nanoscale pores, can be readily obtained by electron irradiation of h-BN. Defects can be studied, as demonstrated, with single-atom precision in direct and real time observation. h-BN layers are an outstanding TEM test platform with easy access to individual B and N atoms. New insights into radiation damage have been presented, and a wealth of further studies is within reach. Finally, BN membranes will allow study of the behavior of adsorbates on its surface by direct TEM observation−similar to graphene−but on a very different, alternative material.

Acknowledgment. We thank Alberto Zobelli for discussions. This work was supported by the German Research Foundation under SFB 569.

Supporting Information Available: Videos showing thinning process of a membrane to a hole, hole growth from vacancies, and formation and removal of a single layer hexagonal boron nitride membrane. This material is available free of charge via the Internet at http://pubs.acs.org.

References

(1) Novoselov, K. S.; Geim, A. K.; Morozov, S. V.; Jiang, D.; Zhang, Y.; Dubonos, S. V.; Grigorieva, I. V.; Firsov, A. A. Electric field effect in atomically thin carbon films. *Science* **2004**, *306*, 666.

(2) Novoselov, K. S.; Jiang, D.; Schedin, F.; Booth, T. J.; Khotkevich, V. V.; Morozov, S. V.; Geim, A. K. Two-dimensional atomic crystals. *Proc. Natl. Acad. Sci.U.S.A.* **2005**, *102*, 10451.

(3) Zhang, Y.; Tan, J. W.; Stormer, H. L.; Kim, P. Experimental observation of the quantum hall effect and berry's phase in graphene. *Nature* **2005**, *438*, 201.

(4) Novoselov, K. S.; Geim, A. K.; Morozov, S. V.; Jiang, D.; Katsnelson, M. I.; Grigorieva, L. V.; Dubonos, S. V.; Firsov, A. A. Two-dimensional gas of massless dirac fermions in graphene. *Nature* **2005**, *438*, 197.

(5) Katsnelson, M. I. Graphene: carbon in two dimensions. *Mater. Today* **2007**, *10*, 20.

(6) Ferrari, A. C.; Meyer, J. C.; Scardaci, V.; Casiraghi, C.; Lazzeri, M.; Mauri, F.; Piscanec, S.; Jiang, D.; Novoselov, K. S.; Roth, S.; Geim, A. K. The raman fingerprint of graphene. *Phys. Rev. Lett.* **2006**, *97*, 187401.

(7) Meyer, J. C.; Geim, A. K.; Katsnelson, M. I.; Novoselov, K. S.; Booth, T. J.; Roth, S. The structure of suspended graphene sheets. *Nature* **2007**, *446*, 60.

(8) Bunch, J. S.; van der Zande, A. M.; Verbridge, S. S.; Frank, I. W.; Tanenbaum, D. M.; Parpia, J. M.; Craighead, H. G.; McEuen, P. L. Electromechanical resonators from graphene sheets. *Science* **2007**, *315*, 490.

(9) Booth, T. J.; Blake, P.; Nair, R. R.; Jiang, D.; Hill, E. W.; Bangert, U.; Bleloch, A.; Gass, M.; Novoselov, K. S.; Katsnelson, M. I.; Geim, A. K. Macroscopic graphene membranes and their extraordinary stiffness. *Nano Lett.* **2008**, *8*, 2442.

(10) Chopra, N. G.; J Luyken, R.; Cherrey, K. C.; Crespi, V. H.; Cohen, M. L.; Louie, S. G.; Zettl, A. Boron nitride nanotubes. *Science* **1995**, *269*, 966.

(11) Loiseau, A.; Willaime, F.; Demoncy, N.; Hug, G.; Pascard, H. Boron nitride nanotubes with reduced numbers of layers synthesized by arc discharge. *Phys. Rev. Lett.* **1996**, *76*, 4737.

(12) Blase, X.; De Vita, A.; Charlier, J.-C.; Car, R. Frustration effects and microscopic growth mechanisms for bn nanotubes. *Phys. Rev. Lett.* **1998**, *80*, 1666.

(13) Bengu, E.; Marks, L. D. Single-walled bn nanostructures. *Phys. Rev. Lett.* **2001**, *86*, 2385.

(14) Lee, R. S.; Gavillet, J.; Lamy de la Chapelle, M.; Loiseau, A.; Cochon, J.-L.; Pigache, D.; Thibault, J.; Willaime, F. Catalyst-free synthesis of boron nitride single-wall nanotubes with a preferred zig-zag configuration. *Phys. Rev. B* **2001**, *64*, 121405R.

(15) Golberg, D.; Bando, Y.; Kurashima, K. Octahedral boron nitride fullerenes formed by electron beam irradiation. *Appl. Phys. Lett.* **1998**, *73*, 2441.

(16) Pokropivny, V. V.; Skorokhod, V. V.; Oleinik, G. S.; Kurdyumov amd, A. V.; Pokropivny, A. V.; Sisonyuk, A. G.; Sheichenko, D. M. Boron nitride analogs of fullerenes (the fulborenes), nanotubes, and fullerites (the fulborenites). *J. Solid State Chem.* **2000**, *154*, 214.

(17) Paetzold, P. New perspectives in boron-nitrogen chemistry. *Pure Appl. Chem.* **1991**, *63*, 345.

(18) Nagashima, A.; Tejima, N.; Gamou, Y.; Kawai, T.; Oshima, C. Electronic structure of monolayer hexagonal boron nitride physisorbed on metal surfaces. *Phys. Rev. Lett.* **1995**, *75*, 3918.

(19) Corso, M.; Auwarter, W.; Muntwiler, M.; Tamai, A.; Greber, T.; Osterwalder, J. Boron nitride nanomesh. *Science* **2004**, *303*, 217.

(20) Han, W.-Q.; Wu, L.; Zhu, Y.; Watanabe, K.; Taniguchi, T. Structure of chemically derived mono- and few-atomic-layer boron nitride sheets. *Appl. Phys. Lett.* **2008**, *93*, 223103.

(21) Pacile, D.; Meyer, J. C.; Girit, C. O.; Zettl, A. The two-dimensional phase of boron nitride: Few-atomic-layer sheets and suspended membranes. *Appl. Phys. Lett.* **2008**, *92*, 133107.

(22) Meyer, J. C.; Girit, C. O.; Crommie, M. F.; Zettl, A. Hydrocarbon lithography on graphene membranes. *Appl. Phys. Lett.* **2008**, *92*, 123110.

(23) Li, J.; Stein, D.; McMullan, C.; Branton, D.; Aziz, M. J.; Golovchenko, J. A. Ion-beam sculpting at nanometre length scales. *Nature* **2001**, *412*, 166.

(24) Meyer, J. C.; Girit, C. O.; Crommie, M.; Zettl, A. Imaging and dynamics of light atoms and molecules on graphene. *Nature* **2008**, *454*, 319.

(25) Spence, J. C. H. *High-Resolution Electron Microscopy*; Oxford University Press: Oxford, 2003.

(26) Lopatin S. Chuvilin A. Unpublished.

(27) Meyer, J. C.; Geim, A. K.; Katsnelson, M. I.; Novoselov, K. S.; Obergfell, D.; Roth, S.; Girit, C.; Zettl, A. On the roughness of single- and bi-layer graphene membranes. *Solid State Commun.* **2007**, *143*, 101.

(28) Krasheninnikov, A. V.; Nordlund, K. Stability of irradiation-induced point defects on walls of carbon nanotubes. *J. Vac. Sci. Technol., B* **2002**, *20*, 728.

(29) Stone, A. J.; Wales, D. J. Theoretical studies of icosahedral c-60 and some related species. *Chem. Phys. Lett.* **1986**, *128*, 501.

(30) Suenaga, K.; Wakabayashi, H.; Koshino, M.; Sato, Y.; Urita, K.; Iijima, S. Imaging active topological defects in carbon nanotubes. *Nat. Nanotechnol.* **2007**, *2*, 358.

(31) Meyer, J. C.; Kisielowski, C.; Erni, R.; Rossell, M. D.; Crommie, M. F.; Zettl, A. Direct imaging of lattice atoms and topological defects in graphene membranes. *Nano Lett.* **2008**, *8*, 3582.

(32) Zobelli, A.; Ewels, C. P.; Gloter, A.; Seifert, G.; Stephan, O.; Csillag, S.; Colliex, C. Defective structure of bn nanotubes: From single vacancies to dislocation lines. *Nano Lett.* **2006**, *6*, 1955.

(33) Liu, L.; Feng, Y. P.; Shen, Z. X. Structural and electronic properties of h-bn. *Phys. Rev. B* **2003**, *68*, 104102.

(34) Zobelli, A.; Gloter, A.; Ewels, C. P.; Seifert, G.; Colliex, C. Electron knock-on cross section of carbon and boron nitride nanotubes. *Phys. Rev. B* **2007**, *75*, 245402.

(35) Seitz, F. Koehler, J. *Solid State Physics* Academic: New York, 1956; Vol. 2.

(36) Azevedo, S.; Kaschny, J. R.; de Castilho, C. M. C.; de Brito Mota, F. A theoretical investigation of defects in a boron nitride monolayer. *Nanotechnology* **2007**, *18*, 495707.
(37) Jimenez, J.; Jankowski, A. F.; Terminello, L. J.; Sutherland, D. G. J.; Carlisle, J. A.; Doll, G. L.; Tong, W. M.; Shuh, D. K.; Himpsel, F. J. Core-level photoabsorption study of defects and metastable bonding configurations in boron nitride. *Phys. Rev. B* **1997**, *55*, 12025.
(38) Kirkland, E. J. *Advanced Computing in Electron Microscopy*; Plenum Press: New York, 1998.
(39) Lichte, H.; Formanek, P.; Lenk, A.; Linck, M.; Matzeck, C.; Lehmann, M.; Simon, P. Electron holography: Applications to materials questions. *Annu. Rev. Mater. Res.* **2007**, *37*, 539.
(40) Giovannetti, G.; Khomyakov, P. A.; Brocks, G.; Kelly, P. J.; Brink, J. v. d. Substrate-induced band gap in graphene on hexagonal boron nitride: Ab initio density functional calculations. *Phys. Rev. B* **2007**, *76*, 073103.

NL9011497